LOCAL PREDICTION OF SUBCOOLED BOILING FLOW IN AN ANNULAR CHANNEL WITH THE INFLUENCE OF BUBBLE COALESCENCE AND BREAK-UP MECHANISMS

G. H. Yeoh[a], J. Y. Tu[b] and Y. Z. Li[c]

a) Australian Nuclear Science and Technology Organisation (ANSTO), PMB 1, Menai, NSW 2234, Australia
b) RMIT University, School of Aerospace, Mechanical and Manufacturing Engineering, PO Box 71, Bundoora, Victoria 3083, Australia
c) School of Energy and Power Engineering, Xi'an Jiaotong University Xi'an, 710049, P. R. China

Abstract

Population balance equations combined with a three-dimensional two-fluid model are employed to predict subcooled boiling flow at low pressure in a vertical annular channel. The MUSIG (MUltiple-SIze-Group) model implemented in CFX4.4 is extended to account for the wall nucleation and condensation in the subcooled boiling regime. Comparison of model predictions against local measurements is made for the void fraction, bubble Sauter diameter and gas and liquid velocities covering a range of different mass and heat fluxes and inlet subcoolings. Good agreement is achieved with the local radial void fraction, bubble Sauter diameter and liquid velocity profiles against measurements. However, significant weakness of the model is evidenced in the prediction of the vapour velocity. Work is in progress to overcome the deficiency of the extended MUSIG model by the consideration of an algebraic slip model to account for bubble separation.

INTRODUCTION

The capability to predict void fraction profile and other two-phase flow parameters in the subcooled boiling region is of considerable importance to nuclear reactor safety. Subcooled boiling flow structure in a research reactor is at low pressures. Because of the critical need to perform safety analysis on a low-pressure research reactor such as HIFAR (HIgh Flux Australian Reactor) and its eventual replacement, the present work concentrates on the development of a boiling model capable of predicting low-pressure subcooled boiling flows.

In our rather comprehensive investigation on axial void fraction distribution in channels, good agreement has been achieved against a wide range of experimental data. Improvements to the boiling flow model in the computational fluid dynamics code - CFX4.4 [1] and the reactor system code - RELAP5 [2] include modifications to inter-phase heat transfer, mean bubble diameter in the bulk liquid, bubble departure diameter relationship and the wall heat transfer process. However, it has been demonstrated following further investigations in [3] that the model predictions against local radial measurements [4] for low-pressure subcooled boiling annular channel flow revealed significant weakness of the model evidenced by the radial prediction of the bubble Sauter diameter, liquid and vapour velocities. The conclusion was that the absence of the bubble mechanistic behaviour such as bubble coalescence clearly observed during experiments in the vicinity of the heated wall significantly compromised the model predictions especially the bubble Sauter diameter distribution.

In the two-fluid model formulation, which describes the most detailed and accurate macroscopic formulation of the thermo-fluid dynamics of the two-phase systems, the phasic interaction terms appear in the field equations. These terms represent the mass, momentum and energy transfers through the interface between the phases. An accurate determination of the bubble Sauter diameter is crucial as the bubble size influences the inter-phase heat and mass transfer through the interfacial area concentrations and momentum drag terms. Another consideration dominating the boiling process as observed in [4] is the occurrence of large bubbles due to the competing mechanisms of bubble coalescence and condensation. In the quest of properly accounting non-uniform bubble size distribution, the implementation of the population balance equations developed by Lo [5], including models developed for predicting bubble coalescence and break-up for adiabatic bubbly flows, is

extended to account for the range of bubble sizes in the subcooled boiling regime. Such a capability does not exist in the current state-of-the-art. Therefore, a successful development of the The MUSIG (MUltiple-SIze-Group) boiling model can contribute to a significant improvement of the two-fluid model formulation for subcooled boiling flows.

The objectives of this present study are therefore to develop the MUSIG boiling model with a complete three-dimensional flow numerical simulation for subcooled boiling flows at low pressures and to evaluate the model through validation against experimental measurements. Comparisons of local quantities for a range of different mass and heat fluxes and inlet subcoolings are performed against recent radial measurements in [4].

MATHEMATICAL FORMULATION

Bubble Coalescence and Break-Up Model

The implementation of population balance equations originally developed by Lo [5] for the generic computer code CFX4.4 is extended to account for the non-uniform bubble size distribution in the subcooled boiling flow regime. In this present study, bubbles ranging from 0mm to 9.5mm diameter are equally divided into 15 classes. Instead of considering 16 different complete phases, it is assumed that each bubble class travels at the same mean algebraic velocity to reduce the computational time. This therefore results in 15 continuity equations for the gas phase coupled with a single continuity equation for the liquid phase.

The break-up of bubbles in turbulent dispersions employs the model developed by Luo and Svendsen [6]. Binary break-up of the bubbles is assumed and the model is based on the theories of isotropic turbulence. For binary breakage, a dimensionless variable describing the sizes of daughter drops or bubbles (the breakage volume fraction) can be defined as

$$f_{BV} = \frac{v_i}{v} = \frac{d_i^3}{d^3} = \frac{d_i^3}{d_i^3 + d_j^3} \tag{1}$$

where d_i and d_j are diameters (corresponding to v_i and v_j) of the daughter particles in the binary breakage of a parent particle with diameter d (corresponding to volume v). The value interval of the breakage volume fraction is between 0 and 1.The break-up rate of bubbles of volume v_j into volume sizes of v_i(= vf_{BV}) can be obtained as

$$\frac{\Omega(v_j : v_i)}{(1-a_g)\, n_j} = C\left(\frac{e}{d_j^2}\right)^{1/3} \int_{x_{min}}^{1} \frac{(1+x)^2}{x^{11/3}} exp\left(-\frac{12 c_f s}{b r_l e^{2/3} d_j^{5/3} x^{11/3}}\right) dx; \quad c_f = \left[f_{BV}^{2/3} + (1-f_{BV})^{2/3} - 1\right] \tag{2}$$

where $x = l/d_j$ is the size ratio between an eddy and a particle in the inertial sub-range and consequently $x_{min} = l_{min}/d_j$; c_f is the increase coefficient of surface area; and C and b are determined respectively to be 0.923 and 2.0 in [6].

The coalescence of two bubbles is assumed to occur in three steps. The first step involves the bubbles colliding trapping a small amount of liquid between them. This liquid film then drains until it reaches a critical thickness and the last step features the rupturing of the liquid film and the bubbles coalesce. The collisions between bubbles may be caused by turbulence, buoyancy and laminar shear. Only the first cause of collision (turbulence) is considered in the present model. Indeed collisions caused by buoyancy cannot be taken into account here as all the bubbles from each class have been assumed to travel at the same speed. Moreover, calculations showed that laminar shear collisions are negligible because of the low superficial gas velocities considered in this investigation. The coalescence rate considering turbulent collision taken from Prince and Blanch [7] can be expressed as

$$c = q_{ij} exp\left(-\frac{t_{ij}}{t_{ij}}\right) \tag{3}$$

where t_{ij} is the contact time for two bubbles given by $\left(d_{ij}/2\right)^{2/3}/e^{1/3}$ and t_{ij} is the time required for two bubbles to coalesce having diameter d_i and d_j estimated to be $\left\{\left(d_{ij}/2\right)^3 r_l/16s\right\}^{1/2}\ln\left(h_0/h_f\right)$. The equivalent diameter d_{ij} is calculated as suggested by Chesters and Hoffman [8]: $d_{ij}=\left(2/d_i+2/d_j\right)^{-1}$. According to [7], for air-water systems, h_0, initial film thickness and, h_f, critical film thickness at which rupture occurs are assumed to be 1×10^{-4}m and 1×10^{-8}m respectively. The turbulent collision rate q_{ij} for two bubbles of diameter d_i and d_j is given by

$$q_{ij}=\frac{p}{4}\left[d_i+d_j\right]^2\left(u_{ti}^2+u_{tj}^2\right);\quad u_{ti}=1.4e^{1/3}d_i^{1/3}\quad\text{and}\quad u_{tj}=1.4e^{1/3}d_j^{1/3} \tag{4}$$

The general form for the population balance equation is

$$\frac{\partial n_i}{\partial t}+\nabla\cdot\left(\vec{u}_g n_i\right)=P_B+P_C-D_B-D_C \tag{5}$$

where P_B, P_C, D_B and D_C are, respectively, the production rates due to break-up and coalescence and the death rate to break-up and coalescence of bubbles. The number density of the ith class n_i is then related to the gas void fraction as $n_i v_i = a_g f_i$.

Flow Equations

The two-fluid model treating both the vapour and liquid phases as continua solves two sets of conservation equations governing mass, momentum and energy, which are written for each phase as:

$$\frac{\partial r_l a_l}{\partial t}+\nabla\cdot\left(r_l a_l\vec{u}_l\right)=\mathrm{G}_{lg}\ \text{- liquid phase} \tag{6}$$

$$\frac{\partial r_g a_g f_i}{\partial t}+\nabla\cdot\left(r_g a_g\vec{u}_g f_i\right)=S_i-f_i\mathrm{G}_{lg}\ \text{- vapour phase} \tag{7}$$

$$\begin{aligned}&\frac{\partial r_k a_k\vec{u}_k}{\partial t}+\nabla\cdot\left(r_k a_k\vec{u}_k\vec{u}_k\right)=-a_k\nabla P+a_k r_k\vec{\mathrm{g}}+\nabla\cdot\left[a_k m_k^e\left(\nabla\vec{u}_k+\left(\nabla\vec{u}_k\right)^T\right)\right]+\\&\sum_{\mathrm{j}=1,\mathrm{j}\neq\mathrm{k}}^{2}\left(\Gamma_{kj}\vec{\mathrm{u}}_j-\Gamma_{jk}\vec{\mathrm{u}}_k\right)+\sum_{\mathrm{j}=1,\mathrm{j}\neq\mathrm{k}}^{2}\mathrm{F}_{kj}\qquad(k,j=1,g)\end{aligned} \tag{8}$$

$$\frac{\partial r_k a_k H_k}{\partial t}+\nabla\cdot\left(r_k a_k\vec{u}_k H_k\right)=Q_k+\nabla\cdot\left[a_k l_k^e\nabla T_k\right]+\sum_{\mathrm{j}=1,\mathrm{j}\neq\mathrm{k}}^{2}\left(\Gamma_{kj}H_j-\Gamma_{jk}H_k\right)\quad(k,j=1,g) \tag{9}$$

In Equation (6), Γ_{lg} represents the mass transfer rate due to condensation in the bulk subcooled liquid, which is expressed by

$$\Gamma_{lg}=\frac{ha_{if}\left(T_{sat}-T_l\right)}{h_{fg}} \tag{10}$$

where h is the inter-phase heat transfer coefficient determined from Ranz and Marshall correlation [9] and a_{if} is the interfacial area per unit volume. The wall vapor generation rate is modelled in a mechanistic way derived by considering the total mass of bubbles detaching from the heated surface:

$$\Gamma_{gl}=\frac{Q_e}{h_{fg}+C_{pl}T_{sub}} \tag{11}$$

where Q_e is the heat transfer due to evaporation. This wall nucleation rate is specified as a boundary condition to Equation (7) and apportioned to the specific discrete bubble class based on the size of the bubble departure diameter on the heated surface. On the right hand side of Equation (7), S_i is the

source term due to coalescence and break-up. The term $f_i \Gamma_{lg}$ represents the mass transfer due to condensation redistributed based on the fraction, f_i, for the discrete bubble classes. Inter-phase transfer terms in the momentum and energy equations – Γ_{kj} and F_{kj} – denote the transfer terms from phase *j* to phase *k*. The mass transfer Γ_{lg} is already given in Equation (10) while the total interfacial force F_{lg} considered in the present study includes the effects of:

$$F_{lg} = F_{lg}^{drag} + F_{lg}^{lift} + F_{lg}^{lubrication} + F_{lg}^{dispersion} \tag{12}$$

where the terms on the right-hand side of Equation (12) are the drag force, lift force, wall lubrication force and turbulent dispersion force respectively. Detail expressions of these forces can be found in Anglart and Nylund [10] and will not be repeated here.

A *k-e* turbulence model is employed for the continuous liquid and dispersed vapor phases. The effective viscosity in the momentum and energy equations is taken as the sum of the molecular viscosity and turbulent viscosity. The turbulent viscosity is considered as the total of the shear-induced turbulent viscosity and Sato's bubble-induced turbulent viscosity [11].

Wall Heat Flux Partition Model

Various experimental and theoretical investigations for low-pressure subcooled boiling flow [12] suggest that the wall heat flux Q_w can be divided into three components: heat transferred due to surface quenching Q_q; heat transferred by evaporation generation Q_e; and heat transferred by turbulent convection Q_c.

The heat transfer due to surface quenching Q_q is determined through the relationship

$$Q_q = \left[\frac{2}{\sqrt{p}} \sqrt{k_l r_l C_{pl}} \sqrt{f} \right] A_q (T_w - T_l) \tag{13}$$

where T_w is the wall temperature and f is the bubble departure frequency given by Kocamustafaogullari and Ishii [13]:

$$f = \frac{1.18}{d_{bw}} \left[\frac{sg\Delta r}{r_l^2} \right]^{0.25} \tag{14}$$

and, A_q, the fraction of wall area subjected to cooling by quenching is calculated from $A_q = N'' \left(p d_{bw}^2 / 4 \right)$. The bubble departure diameter, d_{bw}, and the density of active nucleation sites, N'', are also obtained from [13] expressed by

$$d_{bw} = 2.496 \times 10^{-5} \left(\frac{?_l - ?_g}{?_g} \right)^{0.9} q \left(\frac{s}{g\Delta r} \right)^{1/2} \tag{15}$$

and

$$N'' = \frac{1}{d_{bw}^2} \left[\frac{2s T_{sat}}{(T_w - T_{sat}) r_g h_{fg}} \right]^{-4.4} f(r^*) \tag{16}$$

The bubble contact angle q is taken to be at 40 degrees as suggested in Hsu and Graham [14] for most industrial metals and water. In Equation (16), $r^* = \Delta r / r_g$ and the function $f(r^*)$ is a function of a density ratio described by

$$f(r^*) = 2.157 \times 10^{-7} \, r^{*-3.2} \left(1 + 0.0049 \, r^* \right)^{4.13} \tag{17}$$

The heat flux due to vapor generation at the wall in the nucleate boiling region can be simply calculated from Bowring [15]:

$$Q_e = N'' f\left(\frac{p}{6} d_{bw}^3\right) r_g h_{fg} \tag{18}$$

The heat flux according to the definition of local Stanton number *St* for turbulent convection is:

$$Q_c = St\, r_l C_{pl} u_l (T_w - T_l)(1 - A_q) \tag{19}$$

It is noted that u_l is the local tangential liquid velocity adjacent to the heated surface.

EXPERIMENTAL DETAILS

The experimental rig in [4] consists of a vertical concentric annulus with an inner heating rod of 19mm outer diameter. The heated section is a 1.67m long Inconel 625 tube with 1.5mm wall thickness and is filled with magnesium oxide powder insulation. The rod is uniformly heated by a 54 kW DC power supply. The outer wall is comprised of two stainless steel tubes with 37.5mm inner diameter, which are connected by a transparent glass tube so that visual observation and taking photograph are made possible. The transparent glass tube is 50mm long and is installed just below the measuring plane. The measuring plane is located at 1.61m downstream of the beginning of the heated section. Demineralised water was used as a working fluid. More details regarding the experimental set-up can be found in [4]. The uncertainties of the void fraction and liquid and gas velocity measurements were approximated to be about 3%. However, the uncertainty of the bubble Sauter diameter values was difficult to ascertain and will, at present, be estimated to be lower than 27%. Experimental conditions that have been used for comparison with the simulated results are presented in Table 1. Figure 1 shows the schematic drawing of the test channel.

TABLE 1. Experimental Conditions.

Run	P_{inlet} [Mpa]	T_{inlet} [^{o}C]	T_{sub}(inlet) [^{o}C]	Q_w [kW/m^2]	G [kg/m^{2}s]
C1	0.142	96.6	13.4	152.3	474.0
C2	0.143	92.1	17.9	251.5	1059.2

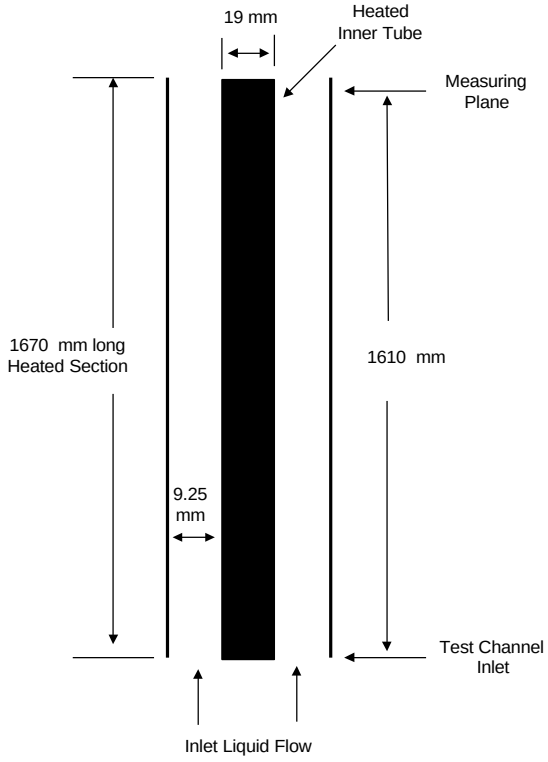

Figure 1. Schematic drawing of the test channel.

NUMERICAL DETAILS

Solution to the two sets of governing equations for the balance of mass, momentum and energy of each phase was sought. The conservation equations were discretised using the control volume technique. The velocity-pressure linkage was handled through the SIMPLE procedure. The discretised equations were solved using Stone's Strongly Implicit Procedure [16]. Since the wall heat flux was applied uniformly throughout the inner wall of the annular and taking advantage of the annular geometrical shape, only a quarter of the annular was considered as the domain for simulation. A body-fitted coordinate system was employed to generate the three-dimensional mesh within the annular channel resulting in a total of 13 (radial) $\times$ 30 (height) $\times$ 3 (circumference) control volumes. Grid independence was examined. In the mean parameters considered, further grid refinement did not reveal significant changes to the two-phase flow parameters. Convergence was achieved within 1500 iterations when the mass residual dropped below 1×10^{-7}. Global execution time on the Silicon Graphics machine was about 30 minutes.

RESULTS AND DISCUSSION

The predicted radial profiles of the bubble Sauter diameter are illustrated in Figure2 while Figure 3 presents the local radial void fraction profiles for experimental conditions of C1 and C2. In all these figures, $(r\text{-}R_i)/(R_o\text{-}R_i)$ = 1 indicates the inner surface of the flow channel wall while $(r\text{-}R_i)/(R_o\text{-}R_i)$ = 0 indicates the surface of the heating rod in the annulus channel.

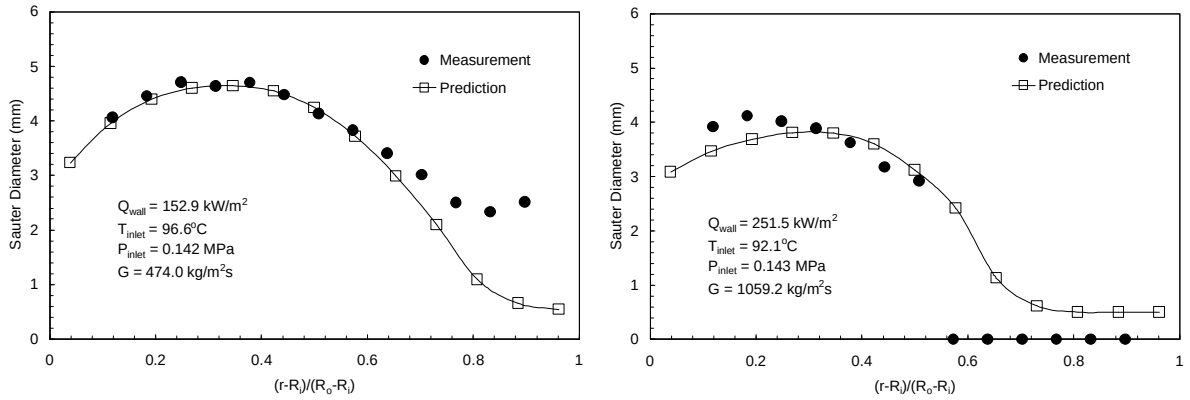

Figure 2. Comparison between predicted and measured radial bubble Sauter profiles for C1 and C2.

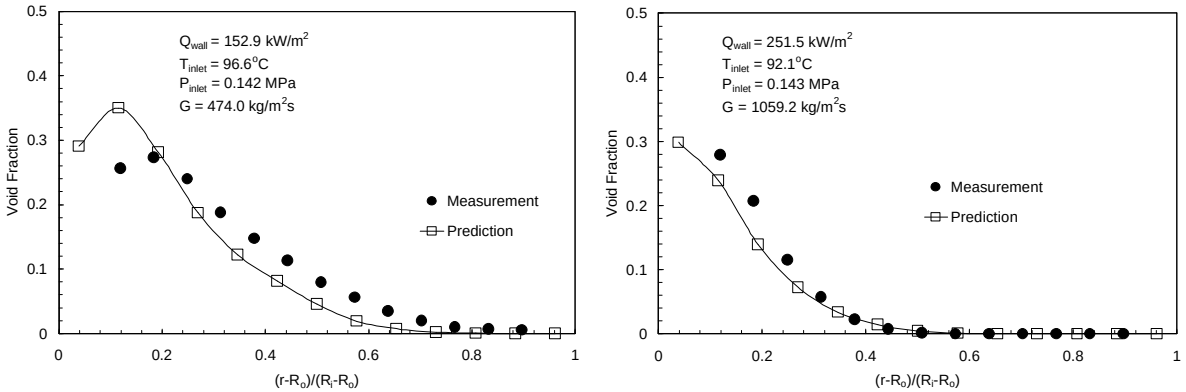

Figure 3. Comparison between predicted and measured radial void fraction profiles for C1 and C2.

At this measuring plane, good agreement is achieved against the experimental values for the bubble Sauter diameter and void fraction profiles. The MUSIG boiling model coupled with the two-fluid model appear to be very promising and present great potential. In subcooled boiling flow, the peak local void fraction is always observed near the heated surface. This high local void fraction found near the heated surface is explicitly due to the large number of bubbles generated from the active nucleation sites on the heated surface. Here, many bubbles are generated from these nucleation sites when the temperature on the heated surface exceeds the saturation temperature. As these bubbles reach a critical size, they

migrate laterally toward the subcooled liquid core under the competing process of bubble coalescence and condensation. The presence of larger bubbles away from the heated wall in Figure 2 succinctly confirmed the merging of bubbles following their departure from the heated surface. The bubble departure diameter evaluated from Equation 15 yielded a size of about 1.3mm. A maximum bubble size was reached of about 4.6mm for C1 and 3.9mm for C2 due to coalescence. The higher mass flux in C2 was found to effectively suppress the coalescence rate thus resulting in a smaller bubble size. It is interesting to note that coalescence of bubbles occurred axially along the heated surface too. The first adjacent points of the simulated results for experimental conditions C1 and C2 predicted a diameter of about 3mm, which was much larger than the bubble departure diameter. Bubbles continually migrating to the subcooled water are subsequently condensed. The bubble Sauter diameter profiles clearly show the gradual collapse of the bubbles and the absence of bubbles near the adiabatic wall of the test channel. Here, only the *low-temperature* single-phase subcooled water existed. The local void fraction also decreases due to condensation. In the subcooled liquid core, more bubbles were condensed in high inlet subcooling condition as shown in C2. The effect of mass flux was the same; as the mass flux increased, interfacial heat transfer was enhanced resulting in more bubbles being condensed in the subcooled liquid core.

The radial profiles of the axial components of local vapour velocity are shown in Figure 4 while Figure 5 present the radial profiles of local liquid velocity for experimental conditions C1 and C2. The vapour velocity is greater than the liquid velocity due to buoyancy force caused by density difference. As observed in the experiment, the vapour velocity was higher at the centre than the velocities near the heating rod. This was probably due to the buoyancy effect being enhanced for the migration of the large bubbles there, which was confirmed by high-speed photography in [4]. However, the vapour velocity predicted by the current boiling model showed higher values approaching the heated boundary. One weakness of the present MUSIG boiling model reflected in Fig. 4 is the assumption that each bubble class travels at the same mean algebraic velocity in order to reduce the computational time and resources. This is however not strictly true. Work is in progress to overcome this deficiency with the development of an algebraic slip model so that bubble separation can be considered. Nevertheless, in Figure 5, the agreement of the liquid velocity with the experimental values at the measuring plane fairs better, showing a closer resemblance to the measurements, in comparison to predicted profiles of the vapour velocity.

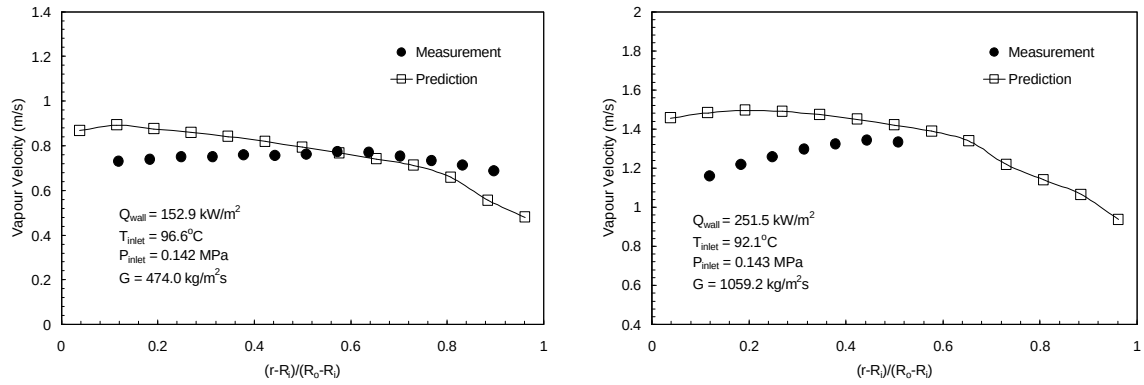

Figure 4. Comparison between predicted and measured radial vapour velocity profiles for C1 and C2.

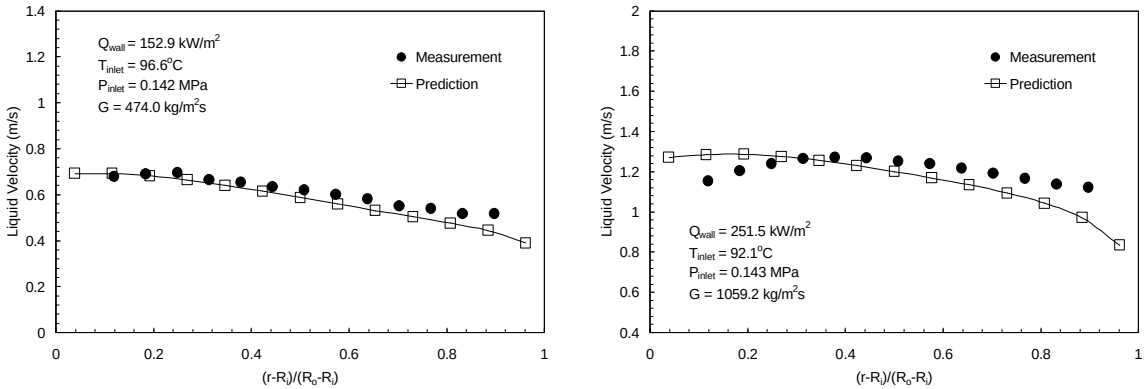

Figure 5. Comparison between predicted and measured radial liquid velocity profiles for C1 and C2.

CONCLUSION

A two-fluid model to predict subcooled boiling flows at low pressures has been coupled with a study of population balance. Bubbles were distributed into 15 diameter classes. Each of them experiencing coalescence and break-up phenomena has been considered. Based on the physical thermal and hydrodynamics of boiling flows, the MUSIG boiling model was principally developed to account for the wall nucleation on the heated surface and condensation in the subcooled liquid core. Comparison of predicted results against local measurements in [4] revealed good agreement for the local radial void fraction, bubble Sauter diameter and liquid velocity profiles. However, based on the assumption that each bubble class travels at the same mean algebraic velocity in order to reduce the computational time and resources, significant weakness of the model is evidenced in the prediction of the vapour velocity. Research is currently ongoing to develop an algebraic slip model to account for bubble separation for a more realistic prediction of the vapour velocity.

REFERENCES

[1] Tu, J. Y. and Yeoh, G. H., 2002a, "On Numerical Modelling of Low-Pressure Subcooled Boiling Flows," *Int. J. Heat & Mass Transfer*, **45**, pp. 1197-1209.

[2] Yeoh, G. H. and J. Y. Tu, 2002b, "Implementation of a Two-Phase Boiling Model into the RELAP/MOD2 Computer Code to Predict Void Distribution in Low-Pressure Subcooled Boiling Flows," *Nucl. Sci. & Eng.*, **140**, pp. 182-188.

[3] Yeoh, G. H., Tu, J. Y., Lee, T. H. and Park, G.-C., 2002c, "Prediction and Measurement of local Two-Phase Flow Parameters in a Boiling Flow Channel*," Num. Heat Transfer: Applications*, **42**, pp. 173-192

[4] Lee, T. H., Park, G.-C. and Lee, D. J., 2002, "Local Flow Characteristics of Subcooled Boiling Flow of Water in a Vertical Annulus," *Int. J. Multiphase Flow*, **28**, pp. 1351-1368.

[5] Lo, S., 1996, "Application of Population Balance to CFD Modelling of Bubbly Flow via the MUSIG model," AEA Technology, *AEAT-1096*.

[6] Luo, H. and Svendsen, H., 1996, "Theoretical Model for Drop and Bubble Break-Up in Turbulent Dispersions," *AIChE J.*, **42**, pp. 1225-1233.

[7] Prince, M. J. and Blanch, H. W., 1990, "Bubble Coalescence and Break-Up in Air-Sparged Bubble Column," *AIChE J.*, **36**, pp. 1485-1499.

[8] Chesters, A. K. and Hoffman, G., 1982, "Bubble Coalescence in Pure Liquids," *Appl. Sci. Res.*, **38**, p.353-361.

[9] Ranz, W. E. and Marshall, W. R., 1952, *Chem. Eng. Prog.*, **48**, pp. 141-148.

[10] Anglart, H. and Nylund, O., 1996, "CFD Application to Prediction of Void Distribution in Two-Phase Bubbly Flows in Rod Bundles," *Nucl. Sci. & Eng.*, **163,** pp. 81-98.

[11] Sato, Y., Sadatomi, M. and Sekoguchi, K., 1981, "Momentum and Heat Transfer in Two-Phase Bubbly Flow-I," *Int. J. Multiphase Flow*, **7**, pp. 167-178.

[12] Judd, R. L. and Hwang, K. S., 1976, "A Comprehensive Model for Nucleate Pool Boiling Heat Transfer Including Microlayer Evaporation," *ASME J. Heat Transfer*, **98**, pp. 623-629.

[13] Kocamustafaogullari, G. and Ishii, M., 1995, "Foundation of the Interfacial Area Transport Equation and its Closure Relations," *Int. J. Heat Mass Transfer*, **38**, pp. 481-493.

[14] Hsu, Y. Y. and Graham, R. W., 1976, *Transport Process in Boiling and Two-Phase Systems*, Hemisphere, Washington.

[15] Bowring, R. W., 1962, "Physical Model Based on Bubble Detachment and Calculation of Steam Voidage in the Subcooled Region of a Heated Channel," *Report HPR-10*, Institute for Atomenergi, Halden, Norway.

[16] Stone, H. L., 1968, "Iterative Solution of Implicit Approximations of Multidimensional Partial Differential Equations," *SIAM J. Num. Analysis*, **5**, pp. 530-558.